Research Square

Preprints are preliminary reports that have not undergone peer review.
They should not be considered conclusive, used to inform clinical practice,
or referenced by the media as validated information.

MAPTAC-Functionalized Poly(acrylic acid-co-sodium acrylate) Hydrogels for Enhanced Pb(II) and Cd(II) Adsorption

Mahdi Taheri
Hamedan University of Technology
Masoud Vesali-Naseh
masood.vesali@gmail.com
Hamedan University of Technology https://orcid.org/0000-0001-6117-6083
Alireza Sabzevari
Meybod University
Kourosh Kabiri
Iran Polymer and Petrochemical Research Institute

Research Article

Keywords: Adsorption, Hydrogel, Poly(acrylic acid-co-sodium acrylate), Heavy metals, MAPTAC

Posted Date: November 6th, 2026

DOI: https://doi.org/10.21203/rs.3.rs-10911089/v1

License: This work is licensed under a Creative Commons Attribution 4.0 International License.
Read Full License

MAPTAC-Functionalized Poly(acrylic acid-co-sodium acrylate) Hydrogels for Enhanced Pb(II) and Cd(II) Adsorption

Mahdi Taheri[1], Masoud Vesali-Naseh[11], Alireza Sabzevari[2], Kourosh Kabiri[3]

[1] Chemical Engineering Department, Hamedan University of Technology, P.O. Box 579-65155, Hamedan, Iran
[2] Biomedical Engineering Department, Meybod University, P.O. Box 8961699557, Meybod, Iran
[3] Adhesive and Resin Department, Iran Polymer and Petrochemical Institute, P.O. Box 14965-115, Tehran, Iran

Abstract

Heavy metals are among the most hazardous environmental pollutants, necessitating the development of efficient materials for their removal from contaminated water. In this study, a poly(acrylic acid-co-sodium acrylate) hydrogel was synthesized and functionalized with 3-(Methacryloylamino)propyltrimethylammonium chloride (MAPTAC). The synthesized hydrogels were characterized using various analytical techniques. Rheological and dynamic mechanical thermal analysis demonstrated that MAPTAC modification enhanced the storage modulus and improved the thermo-mechanical stability of the hydrogel by forming a stronger and more stable polymer network. The modification also reduced the equilibrium swelling capacity while improving the structural integrity of the hydrogel, indicating the formation of a more compact and mechanically stable polymer network. Their adsorption behavior of synthesized hydrogels toward Pb(II) and Cd(II) ions was investigated. Among all formulations, the hydrogel containing 10 g MAPTAC showed the highest adsorption capacities of 118 mg/g for Pb(II) and 117 mg/g for Cd(II), with corresponding removal efficiencies of 94.5% and 94%. Adsorption was systematically evaluated as a function of solution pH, contact time, adsorbent dosage, temperature, and initial metal-ion concentration. The optimal adsorption conditions were pH 6, a contact time of 60 min, a temperature of 25 °C, and an adsorbent dosage of 0.008 g. The equilibrium data were best described by the Freundlich isotherm model, while adsorption kinetics followed the pseudo-second-order model. Thermodynamic analyses indicated that the adsorption process was spontaneous and most favorable at 25 °C. These findings demonstrate that the MAPTAC-functionalized poly(acrylic acid-co-sodium acrylate) hydrogel is an efficient and promising adsorbent for removing Pb(II) and Cd(II) from aqueous media.

Keywords: Adsorption; Hydrogel; Poly(acrylic acid-co-sodium acrylate); Heavy metals; MAPTAC.

1. Introduction

With the rapid growth of the global population and the increasing demand for continuous industrialization, water pollution has become one of the most serious threats to human health and the environment (Lu et al. 2026b). Heavy metals are persistent and hazardous contaminants commonly found in aquatic environments (Monroy-Licht et al. 2025). The major sources of these metals in aquatic environments include battery manufacturing (Lu et al. 2026a),

[1] Corresponding authors: E-mail Address: masood.vesali@gmail.com

electroplating and coating industries (Badsha et al. 2021), metallurgy (Lu et al. 2026b), and pigment-based processes (Zalyhina et al. 2021). Among the various conventional treatment methods, adsorption has proven to be one of the most effective approaches for the removal of heavy metals such as lead and cadmium from wastewater (Kato and Kansha 2024). This technique is particularly advantageous for eliminating contaminants present at low concentrations. Therefore, the development of novel and highly efficient adsorbents for the removal of heavy metals from aqueous environments is of considerable importance (Siahkamari et al. 2017). Polymeric hydrogels have attracted significant attention as soft and functional materials owing to their three-dimensional crosslinked network structure and their remarkable ability to retain large amounts of water (Usman et al. 2023). These materials exhibit excellent hydrophilicity, high swelling capacity, and good biocompatibility and can be produced in large quantities with tunable dimensions(Darban et al. 2022, Rayat Pisheh et al. 2025). The structural characteristics of hydrogels enable controlled swelling and water uptake in aqueous media, making them suitable for a wide range of applications, including agriculture (Kim et al. 2023), regenerative medicine (Rayat Pisheh et al. 2025), biomedical systems (Liu et al. 2018), tissue engineering (Rayat Pisheh et al. 2025), and wastewater treatment (Zhao et al. 2025). Chemical modification of hydrogels through the introduction of functional groups (Alkhaldi et al. 2026) or the incorporation of functional additives, such as graphene (Abdipour et al. 2025) and montmorillonite (Vesali-Naseh et al. 2019), and nanosilica (Mohammadbagheri et al. 2024) can significantly enhance their adsorption performance toward pollutant ions (Badsha et al. 2021). In addition to improving adsorption capacity, these modifications can also enhance key properties, including reusability, stability over a wide pH range, mechanical strength, controlled swelling behavior, and responsiveness to external stimuli (Darban et al. 2022, Zanbili et al. 2025, Chen et al. 2024).

These advantages make hydrogels efficient, cost-effective, and environmentally friendly candidates for industrial wastewater treatment and heavy metal removal (Mohammed et al. 2024). The adsorption mechanisms involved in hydrogels include ion exchange (Fang et al. 2025), electrostatic interactions (Badsha et al. 2021), hydrogen bonding (Ibrahim et al. 2012), surface complexation (Fang et al. 2025), and chelation (Lu et al. 2026b). Acrylate-based hydrogels, particularly poly(acrylic acid), possess a large number of active carboxylic groups, which provide high affinity toward Pb^{2+} and Cd^{2+} ions (Badsha et al. 2021). Furthermore, their modification with functional monomers such as MAPTAC, N-vinylimidazole, and 4-vinylpyridine can increase the number of active adsorption sites and consequently improve the adsorption efficiency (Behrendt et al. 2024).

In the present study, a sodium acrylate-based superabsorbent hydrogel was synthesized and subsequently surface modified with MAPTAC to enhance its adsorption performance. This chemical modification increased both the number and diversity of active adsorption sites, leading to superior adsorption efficiency compared with the unmodified hydrogel. The results of this study demonstrate the high potential of the modified hydrogel for application in industrial wastewater treatment processes and for mitigating heavy metal contamination in aquatic environments.

2. Materials and Methods

2.1. Materials

Ammonium persulfate (APS), MAPTAC, tetramethylethylenediamine (TMEDA), sodium hydroxide (NaOH), acetone, lead nitrate, and cadmium nitrate were purchased from Merck (Germany) and were of analytical grade.

Acrylic acid (AA) and polyethylene glycol dimethacrylate (PEGDMA) were obtained from Sigma-Aldrich (USA). Distilled water was used for the preparation of all solutions and for washing the hydrogel samples.

2.2. Hydrogel synthesis

Synthesis of the poly(acrylic acid-co-sodium acrylate) hydrogel

AA (15 g) was partially neutralized to 75 mol% using an aqueous sodium hydroxide solution prepared by dissolving 6.25 g of NaOH in 20 mL of distilled water. PEGDMA (0.04 g) was added as the crosslinking agent. The APS/TMEDA redox initiator system was subsequently introduced into the reaction mixture, which was stirred at room temperature until the onset of the exothermic polymerization reaction. The concentrations of the monomer, crosslinker, and APS/TMEDA initiator system were 8.3 mol/L, 0.005 mol/L, and 15.5 × 10^{-3} mol/L, respectively.

After polymerization, the resulting hydrogel was removed from the reactor and cut into small pieces. The gel fragments were dried in a forced-air oven at 80 °C for 8 h, ground using a laboratory mill, sieved to obtain the desired particle size, and stored in a desiccator until further use (Fig. 1).

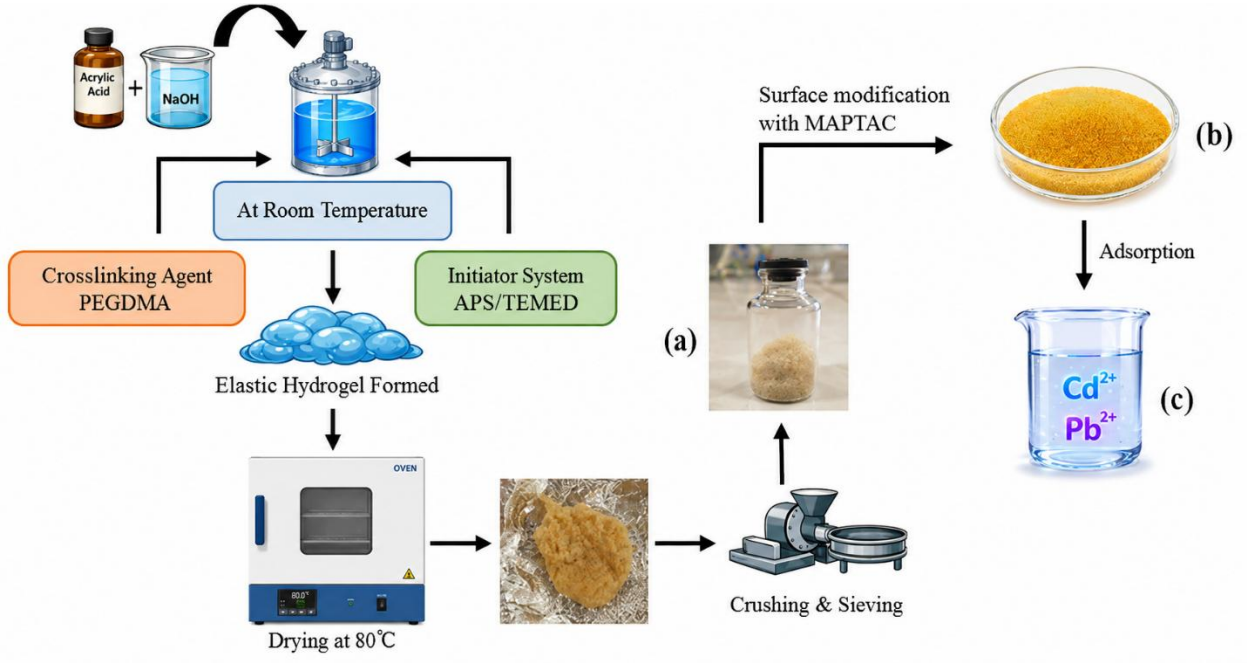


Fig. 1. Schematic representation of (a) base hydrogel synthesis, (b) surface modification, (c) the heavy metal ion adsorption process.

Synthesis of the MAPTAC-modified hydrogel

To evaluate the effect of MAPTAC content on the adsorption performance of the hydrogel, the base poly(acrylic acid-co-sodium acrylate) (PAA) hydrogel was modified using different hydrogel-to- MAPTAC weight ratios (1:1, 1:2, and 1:4, w/w). Briefly, 5 g of the dried hydrogel was mixed with the appropriate amount of MAPTAC. Acetone (5 mL/g hydrogel) was added as the reaction medium to ensure uniform distribution of the monomer within the hydrogel network.

APS/TMEDA was then introduced as the initiator at a hydrogel-to-initiator weight ratio of 1:0.02. Distilled water (0.2 mL/g hydrogel) was added to facilitate mixing and adjust the viscosity of the reaction mixture. The suspension was gently stirred for 1 h to promote the diffusion of MAPTAC into the hydrogel network. The impregnated samples were subsequently heated at 120 °C for 1 h to remove the solvent and promote the grafting/incorporation of MAPTAC into the hydrogel network.

2.3. Characterization

Fourier-transform infrared (FT-IR) spectra were recorded using a PerkinElmer Spectrum spectrometer equipped with an attenuated total reflectance accessory over the wavenumber range of 400–4000 cm^{-1}, with a resolution of 4 cm^{-1} and 32 scans. Dynamic mechanical thermal analysis (DMTA, Mettler Toledo) was performed to evaluate the thermo-mechanical behavior of the adsorbent hydrogels over a temperature range of 25–200 °C at a heating rate of 5 °C min^{-1} and a constant oscillation frequency of 1 Hz. The rheological properties of the synthesized hydrogels were characterized using an Anton Paar Physica MCR 301 rheometer over a frequency range of 0.1–100 Hz. The zeta potential of the samples was measured using a Zetasizer (SZ-100, Horiba Scientific, Japan) to determine the surface charge characteristics of the adsorbents.

2.4. Swelling Properties and Absorbency Under Load

The swelling capacity of the synthesized hydrogels was evaluated in distilled water and 0.9 wt.% NaCl solution. A known mass of the dry hydrogel was immersed in 100 g of the swelling medium and allowed to swell for 1 h until equilibrium was reached.

Swelling behavior was also determined at predetermined time intervals. The equilibrium swelling capacity (Q) was calculated using Eq. (1):

$$Q\left(^{g}/_{g}\right) = \frac{W_s - W_d}{W_d} \qquad (1)$$

where W_s and W_d denote the masses of the swollen and dry hydrogel, respectively. The absorbency under load (AUL) was determined using a cylindrical apparatus equipped with a porous support and subjected to a constant pressure of 0.3 psi. Briefly, 0.1 g of dry hydrogel was uniformly distributed inside the cylinder, and a Teflon piston was placed on top of the sample. The apparatus was then brought into contact with a 0.9 wt.% NaCl solution through a glass filter and maintained for 60 min under load. The swollen sample was subsequently weighed, and the AUL value was calculated using Eq. (2):

$$AUL\left(^{g}/_{g}\right) = \frac{W_2 - W_1}{W_1} \qquad (2)$$

Where W_1 and W_2 represent the weights of the dry and swollen hydrogel under the applied load, respectively.

2.5. Adsorption Experiments

The adsorption performance of the modified hydrogels toward Pb(II) and Cd(II) ions was evaluated in batch experiments. To identify the most effective adsorbent, all MAPTAC-modified hydrogels were initially tested under identical conditions, including a temperature of 25 °C, solution pH of 6, and a contact time of 60 min. In all adsorption experiments, 0.008 g of adsorbent was added to 100 mL of metal ion solution. Among the prepared samples, the hydrogel containing 10 g MAPTAC (hydrogel/MAPTAC ratio of 1:2, w/w) exhibited the highest adsorption capacity and was designated as M10 for subsequent characterization and adsorption studies.

The effects of key operating parameters, including solution pH (2–10), contact time (5–80 min), temperature (5–80 °C), and initial metal ion concentration (10–80 mg/L), were systematically investigated. After adsorption, the suspensions were centrifuged, and the residual concentrations of Pb(II) and Cd(II) ions were determined using atomic absorption spectroscopy (AAS, Agilent 240AA). The adsorption capacity at equilibrium (q_e, mg/g) and removal efficiency (R) were calculated using Eqs. (3) and (4), respectively:

$$q_e = \frac{V(C_0 - C_e)}{m} \quad (3)$$

$$R = \frac{C_0 - C_e}{C_0} \times 100 \quad (4)$$

where C_0 and C_e are the initial and equilibrium concentrations (mg/L), V is the solution volume (L), and m is the mass of adsorbent (g).

2.6. Adsorption Isotherm and Kinetic Modeling

To elucidate the adsorption equilibrium, mechanism, and possible rate-controlling steps of Pb(II) and Cd(II) removal by the hydrogel, the experimental data were analyzed using the Langmuir, Freundlich, Temkin, Dubinin–Radushkevich (D–R), and Sips isotherm models, together with the pseudo-first-order (PFO), pseudo-second-order (PSO), Weber–Morris intraparticle diffusion, and Elovich kinetic models. The parameters of each model were obtained by nonlinear regression analysis of experimental data. The corresponding equations and model parameters are summarized in Table 1. The goodness of fit of each model was assessed based on the coefficient of determination (R^2).

Table 1. Isotherm and kinetic models employed for adsorption analysis.

Isotherm model	Isotherm equation	Kinetic model	Kinetic equation
Langmuir	$q_e = \frac{q_m K_L C_e}{1 + K_L C_e}$	PFO	$q_t = q_e(1 - e^{-K_1 t})$
Freundlich	$q_e = K_F C_e^{1/n}$	PSO	$q_t = \frac{K_2 q_e^2}{1 + K_2 q_e t}$
Temkin	$q_e = B\ln(K_T C_e)$	Weber –Morris	$q_t = K_{id}.t^{0.5} + C$
D-R	$q_e = q_m \exp(-\beta_{DR}\varepsilon^2)$, $\varepsilon = RT\ln(1 + \frac{1}{C_e})$	Elovich	$q_t = \frac{1}{\beta_E}\mathrm{Ln}(\alpha\beta_E) + \frac{1}{\beta_E}\mathrm{Ln}(t)$
Sips	$q_e = \frac{q_m K_S C_e^n}{1 + K_s C_e^n}$		

q_e: equilibrium adsorption capacity (mg/g), q_m: maximum adsorption capacity of the adsorbent (mg/g), K_L, K_F, K_T, K_S: isotherm constants, n: Freundlich adsorption intensity parameter, B: Temkin constant, β_{DR}: D–R isotherm constant related to the mean adsorption energy, R: universal gas constant, T: absolute temperature (K), q_t: adsorption capacity

at time t (mg/g), K_1, K_2: rate constants, K_{id}: intraparticle diffusion rate constant (mg/g.min$^{0.5}$), C: intercept, α: initial adsorption rate (mg/g.min), β_E: Elovich constant related to surface coverage and chemisorption activation energy (g /mg).

2.7. Thermodynamic Studies

The thermodynamic behavior of the adsorption process was investigated by determining the standard Gibbs free energy change (ΔG°), enthalpy change (ΔH°), and entropy change (ΔS°). The thermodynamic equilibrium constant (K) was calculated at different temperatures, and the values of ΔH° and ΔS° were obtained from the slope and intercept of the Van't Hoff plot (ln K versus 1/T), respectively [16]. The equations used for thermodynamic calculations are presented in Table 2.

Table 2. Thermodynamic models, equations, and associated parameters.

Description	Equation
Equilibrium constant	$K = \frac{q_e}{C_e} \times M$
Gibbs free energy	$\Delta G^{\circ} = -RT\ln(K)$
Van't Hoff equation	$\ln(K) = \frac{\Delta S^{\circ}}{R} - \frac{\Delta H^{\circ}}{RT}$
Thermodynamic relation	$\Delta G^{\circ} = \Delta H^{\circ} - T\,\Delta S^{\circ}$

M represents the adsorbent dosage (g/L) used to convert the distribution coefficient into a dimensionless equilibrium constant for thermodynamic calculations.

3. Results and Discussion

3.1. FT-IR Analysis

Figure 2 presents the FT-IR spectra of the PAA and M10 hydrogels before adsorption and of M10 after Pb^{2+} and Cd^{2+} adsorption. As shown in Fig. 2a, MAPTAC incorporation resulted in noticeable changes in the intensity and profile of the characteristic absorption bands of PAA, particularly in the O–H stretching and carbonyl/carboxylate regions, supporting the successful modification of the polymer network (Vesali-Naseh et al. 2019). After metal adsorption (Fig. 2b,c), further changes in band intensity and shape were observed, particularly in the 3000–3600 cm^{-1} and 1400–1800 cm^{-1} regions, indicating alterations in the chemical environment of the functional groups involved in adsorption (Naderzadeh et al. 2026, Liu et al. 2018).

The broad O–H stretching band at 3000–3600 cm^{-1} decreased in intensity and broadened after adsorption, suggesting changes in the hydrogen-bonding environment. Changes in the C–H stretching region (2800–3000 cm^{-1}) may also reflect alterations in the local chemical environment of the polymer chains following metal adsorption. The variations observed in the carbonyl and carboxylate bands are consistent with the involvement of oxygen-containing functional groups in Pb^{2+} and Cd^{2+} binding (Xu et al. 2024). Changes in the C–O and C–N regions (1000–1300 cm^{-1}) further support modifications in the local environment of the polymer functional groups after adsorption (Siahkamari et al.

2017). Additional changes below 700 cm^{-1} may be associated with changes in the vibrational environment following metal adsorption (Hu et al. 2024). Overall, the FT-IR results support the successful incorporation of MAPTAC into the PAA network and indicate that oxygen-containing functional groups play an important role in Pb^{2+} and Cd^{2+} binding. The observed spectral changes after adsorption are consistent with the involvement of chemical interactions in the adsorption process (Hu et al. 2024).

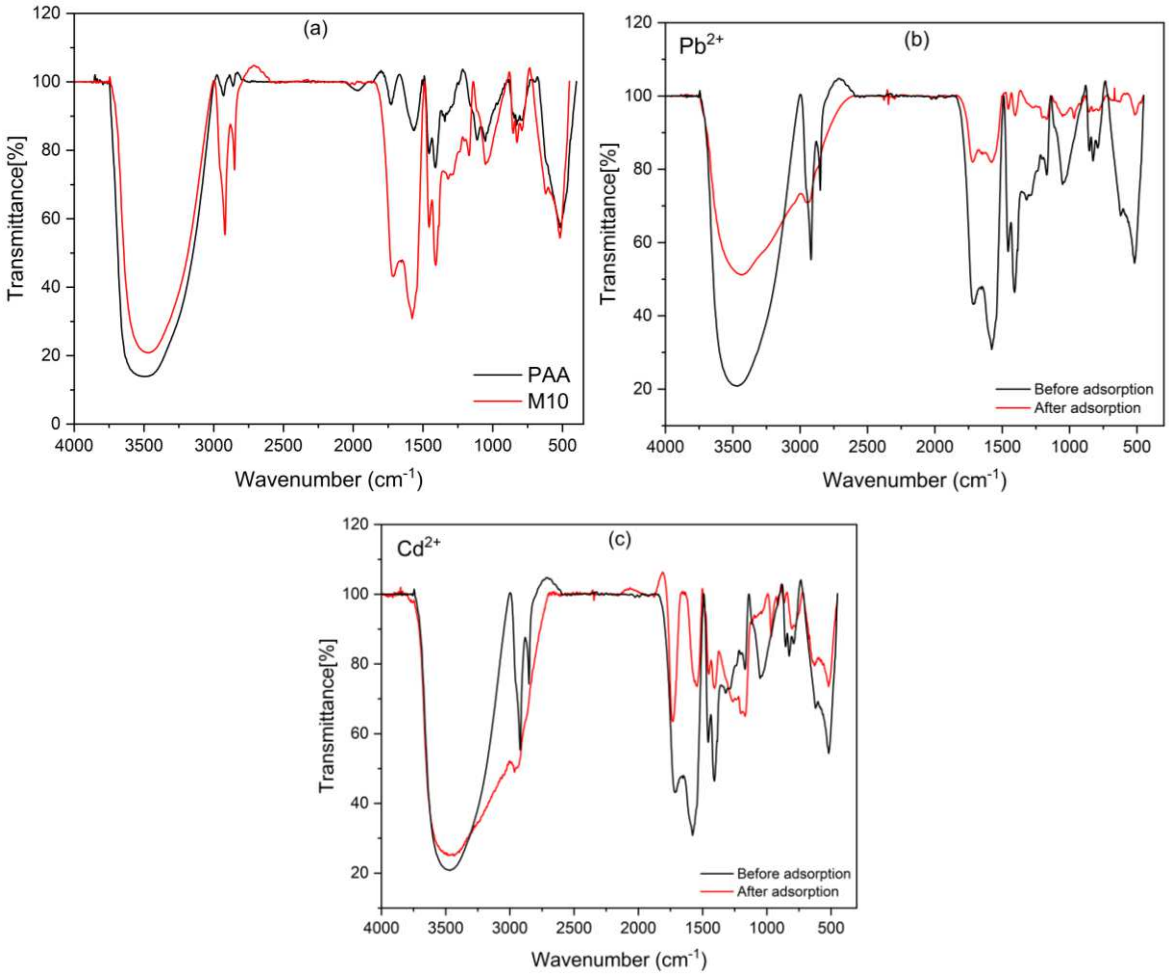


Fig. 2. FT-IR spectra of (a) PAA and M10 hydrogels before adsorption, and M10 before and after adsorption of (b) Pb^{2+} and (c) Cd^{2+} ions.

3.2. DMTA Results

According to the DMTA curves presented in Fig. 3a, the storage modulus (E′), exhibited an initial value of approximately 10,500 kPa at room temperature, indicating high initial stiffness and restricted chain mobility in the poly(acrylic acid) network crosslinked with PEGDMA. As the temperature increased, E′ gradually decreased, and a distinct peak appeared in the tan δ curve around 81 °C, corresponding to the glass transition temperature (T_g) of the PAA polymer network. Beyond T_g, a significant reduction in E′ was observed, reaching nearly 4.2 MPa at

approximately 120 °C. This behavior indicates the transition of the hydrogel into the rubbery region, accompanied by enhanced segmental motion of the polymer chains.

The DMTA results suggest that PEGDMA provided effective crosslinking within the polymer network. Furthermore, The T_g value around 81 °C indicates that the hydrogel remains in a glassy and mechanically stable state under typical wastewater treatment temperatures (< 40 °C) (Kim et al. 2023).

In the M10 sample, the initial E′ was higher than that of the PAA hydrogel, indicating greater initial stiffness. This enhancement may be attributed to additional intermolecular interactions involving the quaternary ammonium groups of MAPTAC and carboxyl groups in the PAA network. With increasing temperature, E′ decreased more gradually than in PAA, indicating improved mechanical stability after modification. The tan δ peak for M10 appeared at approximately 84 °C, indicating a slight increase in T_g. This shift may be associated with increased network interactions that restrict segmental mobility (Furtado et al. 2023). The modified hydrogel retained a higher storage modulus throughout the temperature range, demonstrating improved structural integrity and thermomechanical stability compared with PAA.

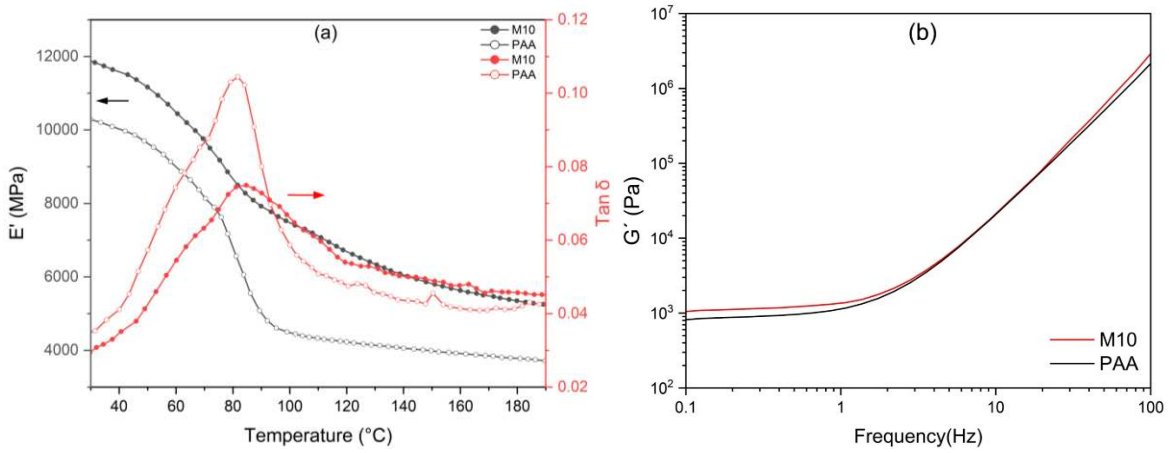


Fig. 3. (a) DMTA curves and (b) storage modulus for PAA and M10 hydrogels.

3.3. Rheological Analysis

Figure 3b presents the frequency dependence of the storage modulus (G′) for the PAA and M10 hydrogels. The G′ values of the M10 hydrogel are consistently higher than those of the PAA over the entire frequency range, indicating the formation of a stronger and more elastic polymer network after modification. This enhancement may be attributed to the formation of a more interconnected polymer network upon MAPTAC incorporation. The difference between the two samples is more pronounced at low frequencies, where polymer chains have sufficient time to rearrange and relax under the applied deformation. This behavior suggests enhanced network integrity and stronger intermolecular interactions in the modified hydrogel. As the frequency increases, both samples exhibit a similar increase in G′, and the gap between the curves gradually decreases. At high frequencies, the deformation time becomes too short for significant chain relaxation, resulting in a predominantly elastic response and more similar rheological behavior (Furtado et al. 2023, Deptula et al. 2023). These results are consistent with the DMTA findings and confirm the formation of a more cohesive and robust polymer network following MAPTAC incorporation (Liu et al. 2018).

3.4. AUL Results

Figure 4 illustrates the effect of MAPTAC content on the AUL of the PAA and M10 hydrogels. The pristine PAA sample exhibited the lowest AUL value, indicating limited resistance to external pressure. Under compressive load, the relatively weak network partially collapsed, reducing its structural integrity and water-retention capacity. The increase in AUL with MAPTAC content indicates improved network strength and structural integrity. This improvement may be attributed to stronger intermolecular interactions and improved network integrity resulting from the incorporation of MAPTAC (Kim et al. 2023). Further increasing the MAPTAC content to 20 g resulted in only a slight increase in AUL, suggesting that the reinforcing effect approached saturation. Excessive MAPTAC incorporation likely produced a more rigid network with reduced chain flexibility, limiting further improvements in absorbency. Although PAA–MAPTAC (20 g) exhibited a slightly higher AUL, the improvement compared with PAA–MAPTAC (10 g) was marginal (Fei et al. 2023).

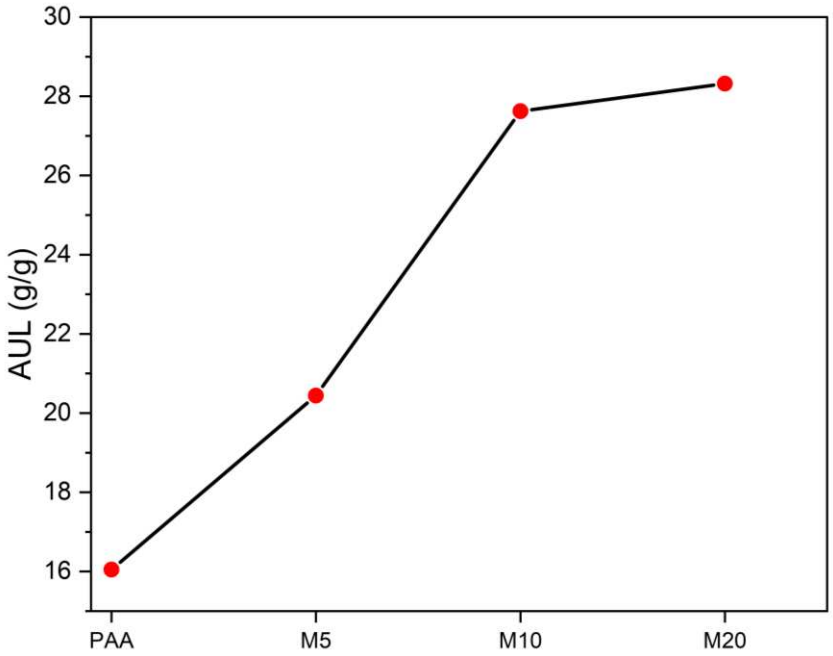


Fig. 4. Effect of MAPTAC content on the AUL of PAA and PAA–MAPTAC hydrogels.

3.5. Swelling Behavior

Based on the AUL results, the swelling behavior of PAA and M10 hydrogels was evaluated in distilled water and 0.9 wt.% NaCl solution (Fig. 5). In distilled water, the PAA hydrogel exhibited the highest swelling capacity, reaching equilibrium after approximately 60 min. This high swelling capacity is attributed to the strong osmotic pressure generated by ionized carboxyl groups within the polymer network (Fei et al. 2024). In comparison, the M10 hydrogel showed a lower equilibrium swelling capacity, which is attributed to MAPTAC incorporation that enhances network cohesion and restricts polymer chain expansion (Linder et al. 2024).

A similar trend was observed in the saline solution, where the swelling capacity of both hydrogels decreased markedly due to the ionic screening effect of Na^+ ions, which reduces electrostatic repulsion between charged groups and suppresses network expansion (Fei et al. 2024).

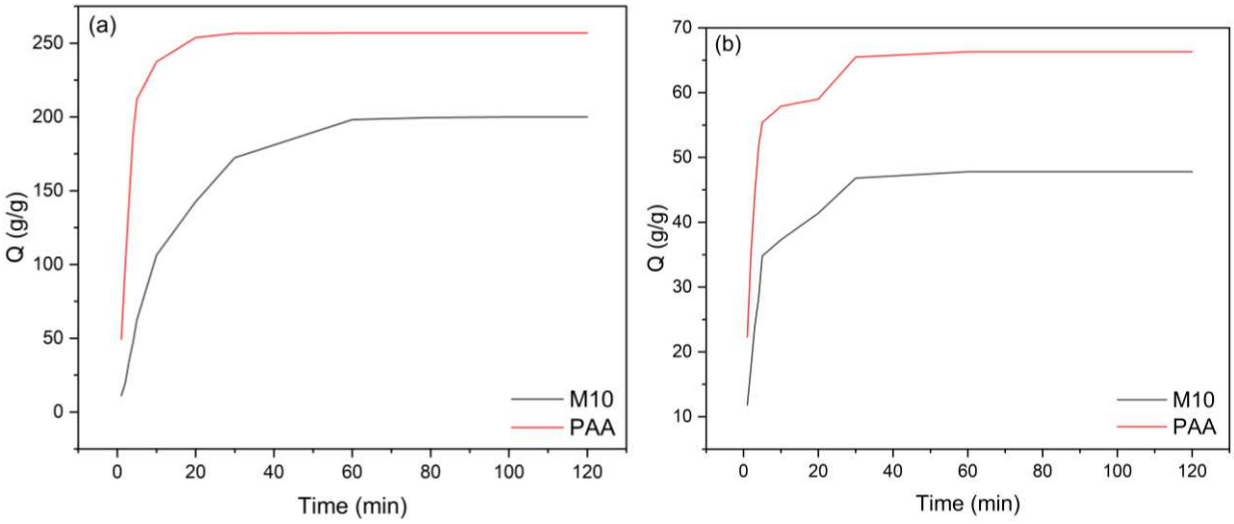


Fig. 5. Free swelling behavior of PAA and M10 hydrogels in (a) distilled water and (b) 0.9 wt.% NaCl solution.

3.6. Zeta Potential Analysis

The surface charge properties of the PAA and M10 hydrogels were investigated by zeta potential measurements at different pH values (Fig. 6). For the PAA hydrogel, the zeta potential decreased with increasing pH, with the isoelectric point located near pH 4. This behavior is attributed to the progressive deprotonation of carboxylic acid groups, resulting in the formation of negatively charged carboxylate groups at higher pH values (Xu et al. 2024). A similar trend was observed for the M10 hydrogel; however, the magnitude of the zeta potential was considerably higher. Although both hydrogels exhibited similar isoelectric points, the M10 sample showed a broader zeta potential range, reflecting the presence of additional ionizable functional groups. The higher positive charge under acidic conditions is likely associated with the protonation of nitrogen-containing functional groups introduced by MAPTAC. At alkaline pH, the more negative zeta potential may be attributed to increased deprotonation of carboxylate groups within the modified polymer network. The more negative surface charge of M10 at pH 6 may favor the adsorption of divalent metal ions by enhancing electrostatic attraction (Yang et al. 2021, Zhao et al. 2025).

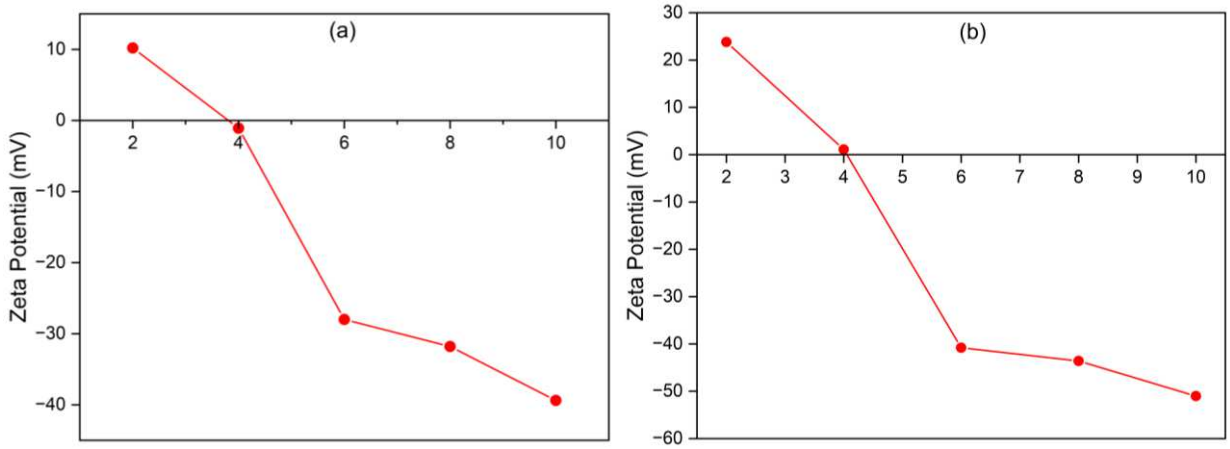


Fig. 6. Zeta potential of (a) PAA and (b) M10 hydrogels as a function of solution pH.

3.7. Effect of operating parameters

Initial metal ion concentration

The effect of initial metal ion concentration on the adsorption performance of PAA and M10 hydrogels is shown in Fig. 7. The q_e increased with increasing initial concentration for both Pb^{2+} and Cd^{2+} ions, which can be attributed to the higher driving force for mass transfer and increased collision frequency between metal ions and available adsorption sites (Xu et al. 2024). In contrast, R decreased with increasing initial concentration because the number of metal ions exceeded the finite adsorption capacity of the hydrogel, leading to progressive saturation of the available adsorption sites (Foo and Hameed 2010).

The M10 hydrogel exhibited higher q_e and R values than PAA over the entire concentration range, reflecting the contribution of the additional cationic ammonium groups introduced by MAPTAC to metal-ion binding (Badsha et al. 2021). Furthermore, Pb^{2+} showed higher adsorption capacities than Cd^{2+} for both hydrogels, likely due to its stronger affinity toward the oxygen- and nitrogen-containing functional groups in the polymer network (Zhao et al. 2025).

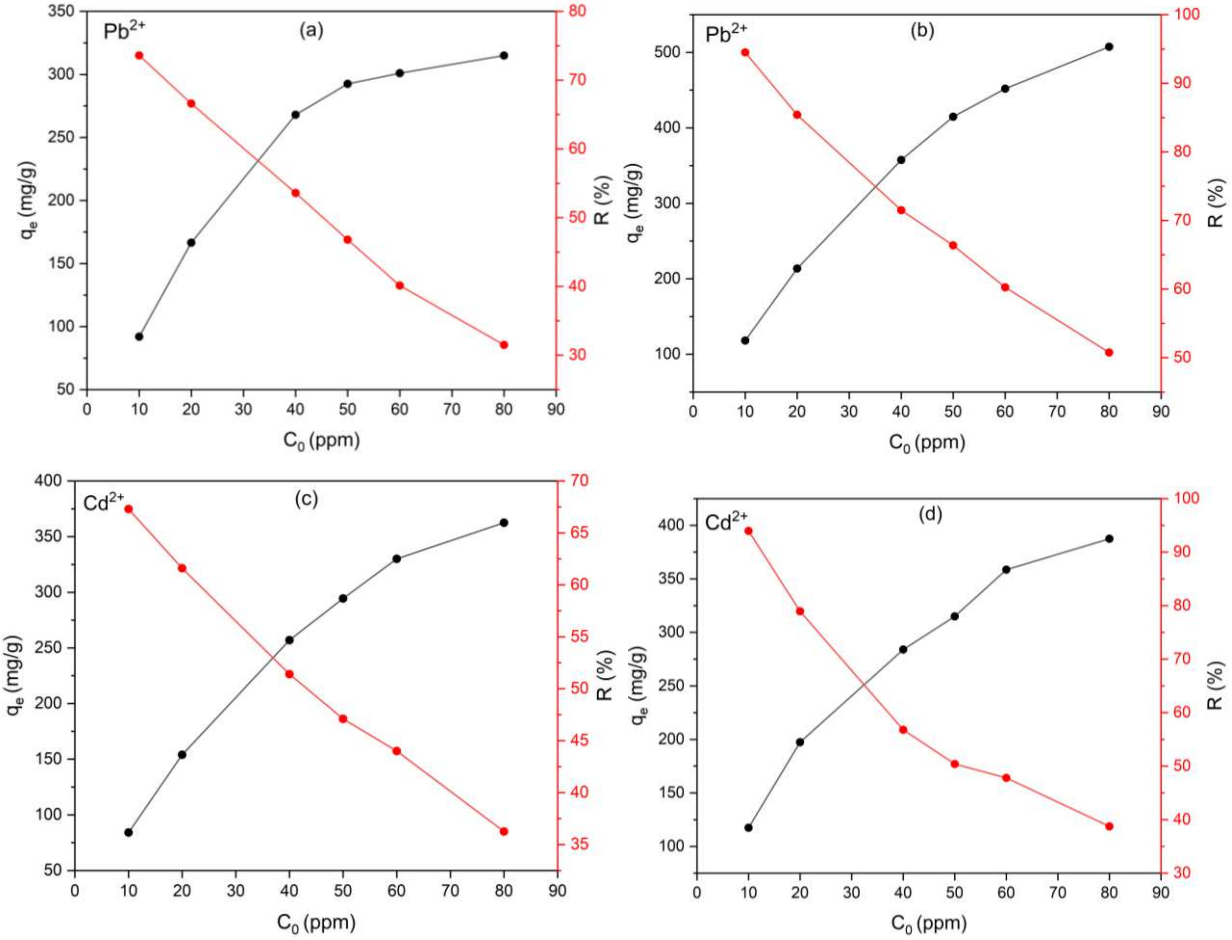


Fig. 7. Effect of initial metal-ion concentration on the adsorption capacity and removal efficiency of Pb(II) and Cd(II) ions by (a, c) PAA and (b, d) M10 hydrogels.

Adsorbent Dosage

Figure 8 shows the influence of adsorbent dosage on the adsorption of Pb^{2+} and Cd^{2+} ions by PAA and M10 hydrogels. M10 consistently exhibited higher adsorption performance than PAA for both Pb^{2+} and Cd^{2+} ions. Increasing the

adsorbent dosage from 0.004 to 0.016 g resulted in a decrease in q_e, while R increased up to an optimum dosage of 0.008 g, beyond which no significant improvement was observed and, in some cases, decreased slightly.

The decrease in q_e with increasing dosage is attributed to the lower amount of metal ions available per unit mass of adsorbent (Zhao et al. 2025). The limited improvement in R at higher dosages may be associated with particle aggregation and overlap of adsorption sites, which reduce the effective surface area and accessibility of active sites (Zhao et al. 2025). Accordingly, 0.008 g was selected as the optimum adsorbent dosage for subsequent adsorption experiments.

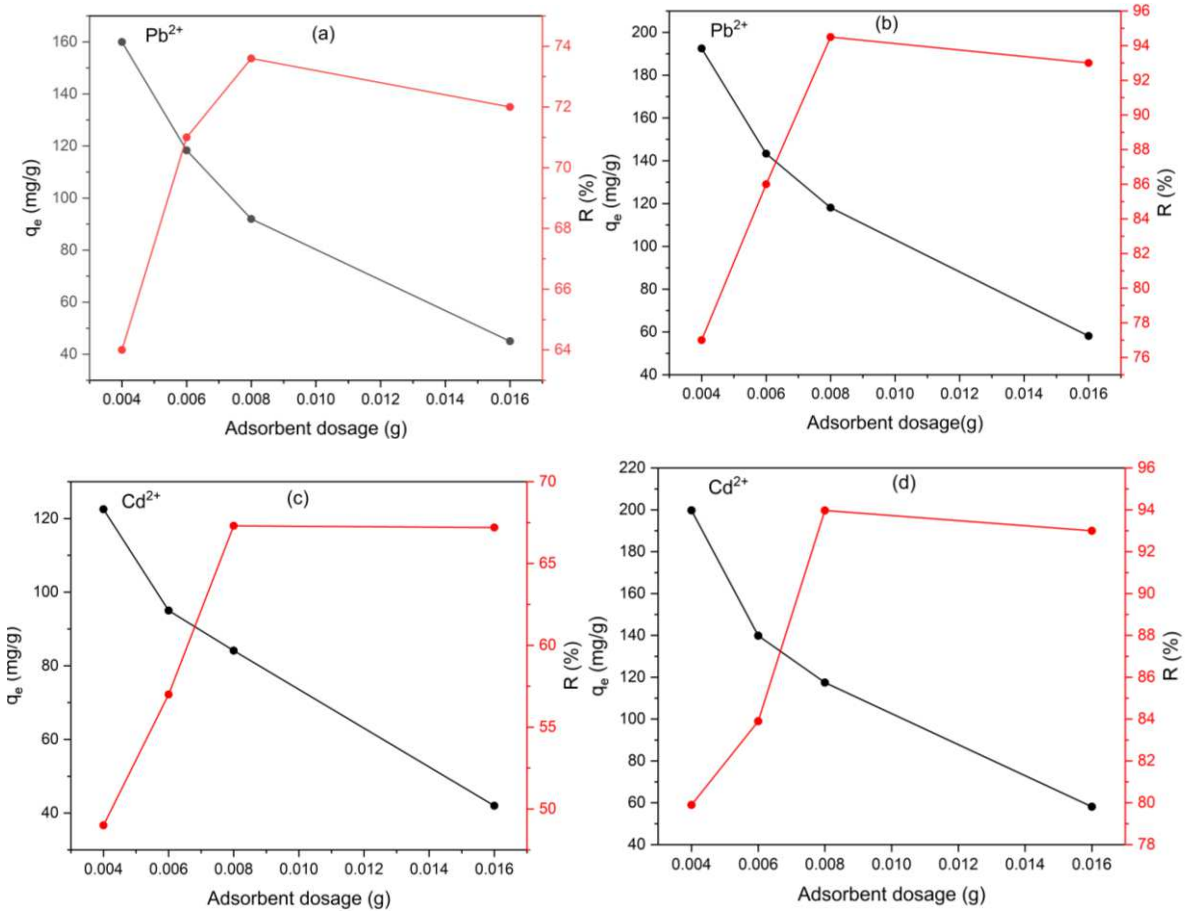


Fig. 8. Effect of adsorbent dosage on the adsorption capacity and removal efficiency of Pb^{2+} and Cd^{2+} ions using (a, c) PAA and (b, d) M10 hydrogels.

Effect of pH

Figure 9 presents the effect of solution pH on the adsorption of Pb^{2+} and Cd^{2+} ions by PAA and M10 hydrogels. Both q_e and R were strongly pH-dependent. At acidic pH values (2–4), relatively low adsorption was observed, which can be attributed to the protonation of carboxyl and amino functional groups and the resulting competition between H^+ and metal ions for available adsorption sites (Zhao et al. 2025). As the pH increased, adsorption improved and reached a maximum at pH 6, where progressive deprotonation of the functional groups resulted in a more negatively charged surface and enhanced electrostatic attraction toward Pb^{2+} and Cd^{2+} (Badsha et al. 2021). The M10 hydrogel exhibited

higher q_e and R values than PAA, which may be associated with the structural and surface modifications induced by MAPTAC incorporation (Badsha et al. 2021).

At alkaline pH values, the adsorption profiles showed a non-monotonic trend, with partial recovery in both q_e and R at pH 10. This behavior may result from the combined effects of increased deprotonation of the functional groups, which favors metal-ion binding, and the partial precipitation of Pb(II) and Cd(II) hydroxides, which can also contribute to the measured metal removal. Therefore, the apparent adsorption performance at high pH cannot be attributed exclusively to adsorption by the hydrogel. Accordingly, pH 6 was selected as the optimum adsorption pH, as it provided high adsorption performance while minimizing the possible contribution of metal hydroxide precipitation (Takeda et al. 2024).

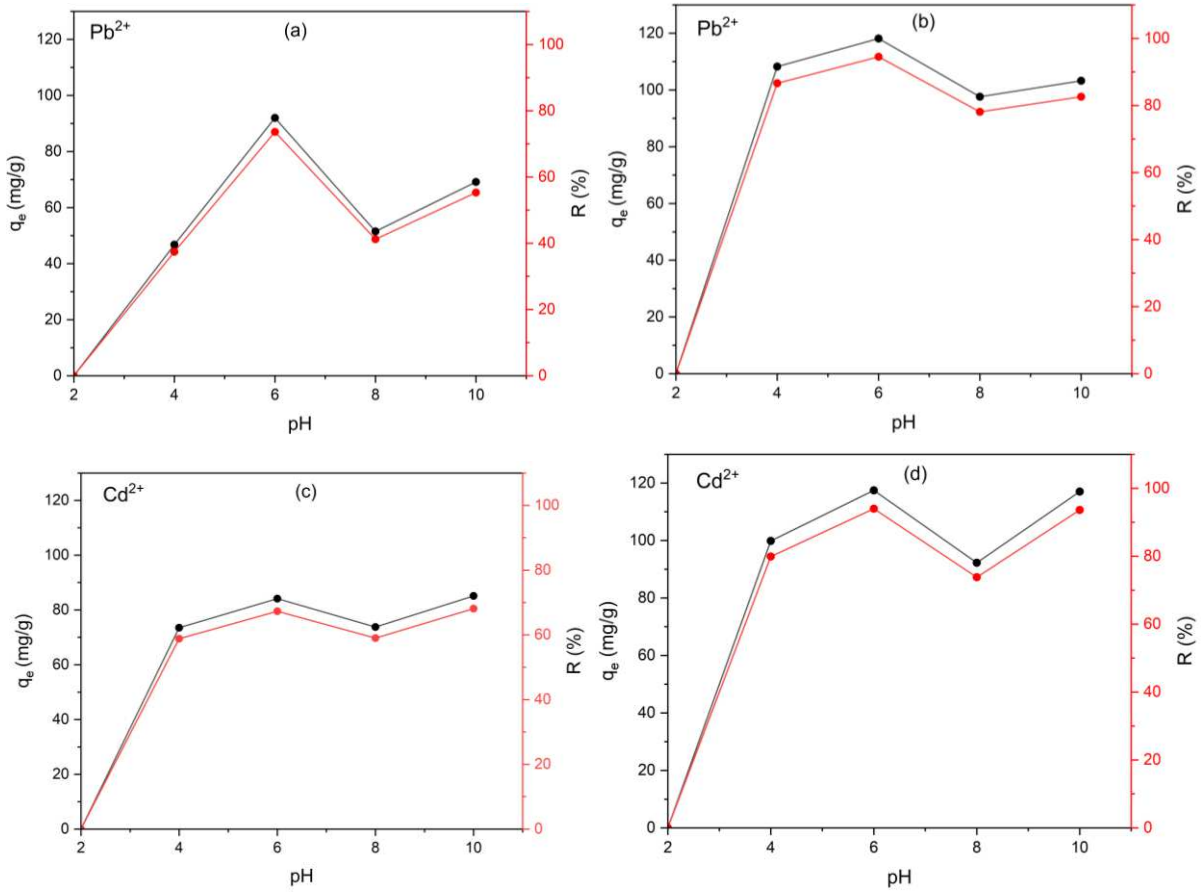


Fig. 9. Effect of pH on the adsorption capacity and removal efficiency of Pb(II) and Cd(II) ions by (a, c) PAA and (b, d) M10 hydrogels.

Effect of Contact time

The influence of contact time on the adsorption of Pb^{2+} and Cd^{2+} ions by PAA and M10 hydrogels is presented in Fig. 10. Both the adsorption capacity and removal efficiency increased rapidly during the initial stages, owing to the abundance of available active sites and the high concentration gradient between the solution and adsorbent surface. As contact time further increased, the adsorption rate gradually decreased due to progressive occupation of the active sites, and equilibrium was reached after approximately 60 min (Zhao et al. 2025). Beyond this point, both parameters

remained nearly constant, with only slight fluctuations that may be attributed to adsorption–desorption equilibrium or experimental variation. The M10 sample exhibited higher adsorption performance than PAA, reflecting the contribution of MAPTAC to metal-ion binding. Accordingly, 60 min was selected as the optimum contact time for subsequent experiments.

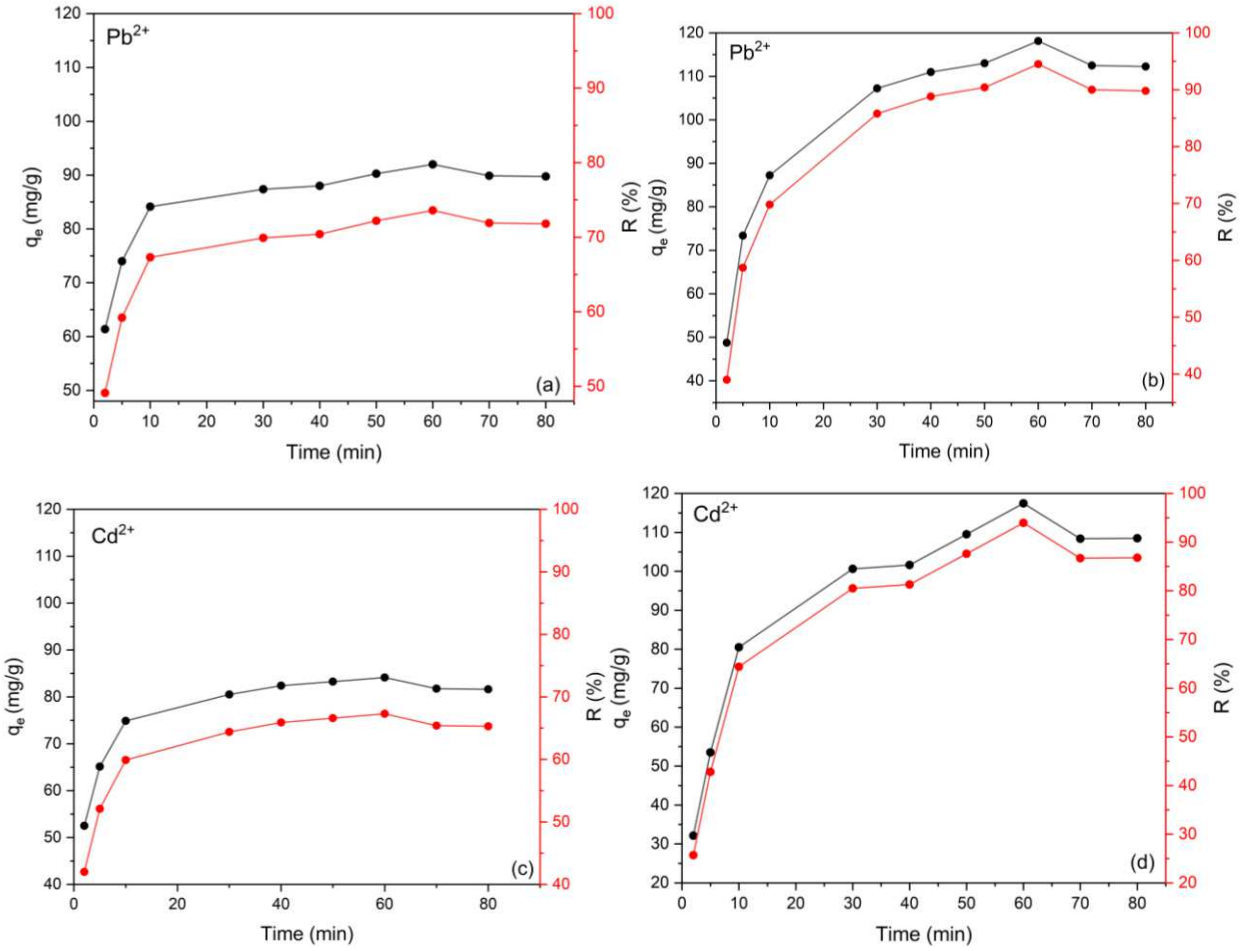


Fig. 10. Effect of contact time on the adsorption capacity and removal efficiency of Pb(II) and Cd(II) ions by (a, c) PAA and (b, d) M10 hydrogels.

Effect of Temperature

Figure 11 shows the effect of temperature on the adsorption of Pb^{2+} and Cd^{2+} ions by PAA and M10 hydrogels. Both q_e and R increased with temperature up to 25 °C and subsequently decreased at higher temperatures. For Pb^{2+}, the q_e values of both PAA and M10 increased up to 25 °C and subsequently decreased at higher temperatures, with M10 consistently showing higher adsorption capacity than PAA. A similar trend was observed for Cd^{2+}, with the maximum q_e and R values obtained at 25 °C for both hydrogels. The M10 hydrogel exhibited higher q_e and R values than PAA throughout the investigated temperature range.

The initial increase in adsorption performance can be attributed to enhanced metal-ion diffusion and reduced mass-transfer resistance at moderate temperatures, facilitating access to active adsorption sites within the hydrogel network

(Badsha et al. 2021). At higher temperatures, the decreases in both q_e and R suggest less favorable adsorption, possibly due to weakened adsorbent–metal interactions and an increased tendency for desorption.

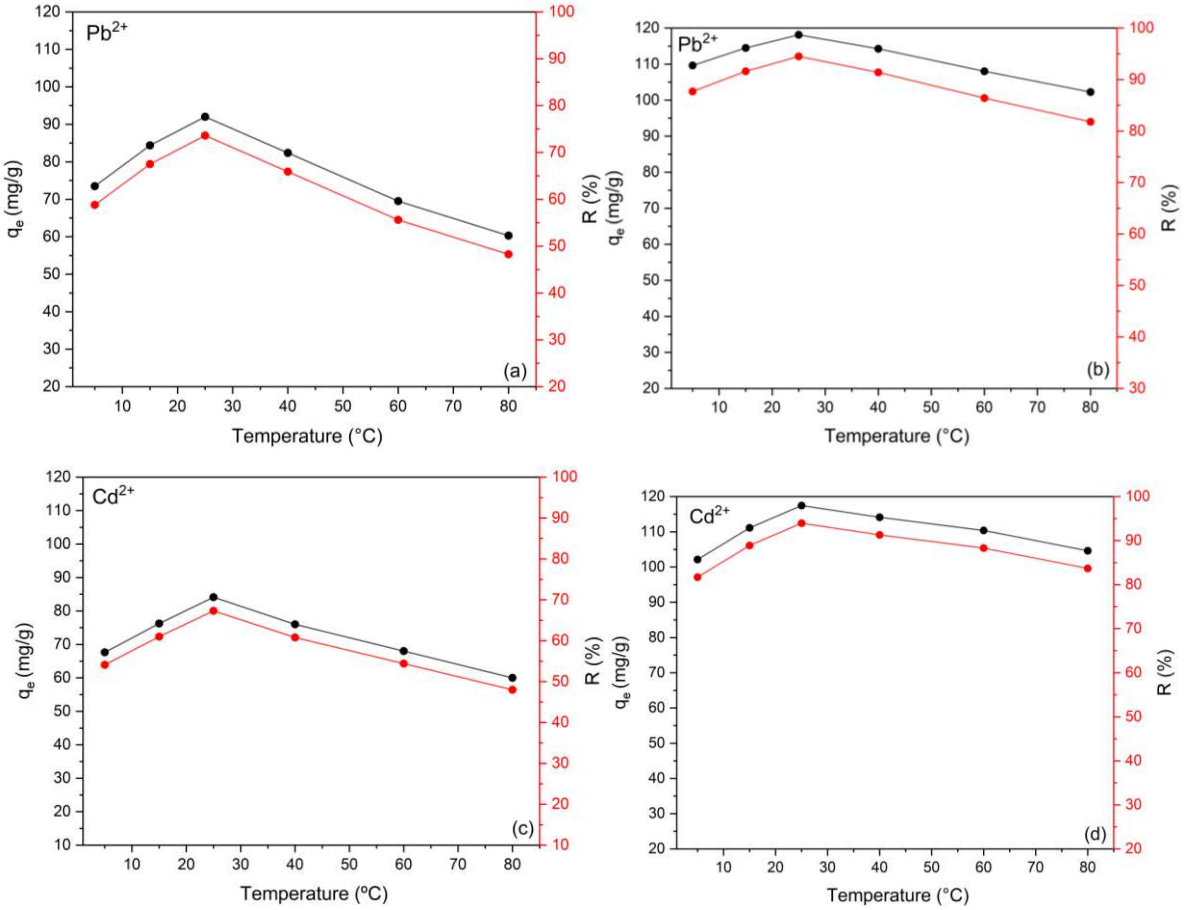


Fig. 11. Effect of temperature on the adsorption capacity and removal efficiency of Pb(II) and Cd(II) ions by (a, c) PAA and (b, d) M10 hydrogels.

3.8. Adsorption Isotherms

Nonlinear fitting curves for the adsorption equilibrium of Pb^{2+} and Cd^{2+} ions onto PAA and M10 hydrogels are presented in Fig. 12, and the corresponding fitted parameters are summarized in Table 3. For both adsorbents, the adsorption capacity increased with increasing C_e and gradually approached saturation, indicating progressive occupation of the available adsorption sites. The M10 hydrogel consistently exhibited higher equilibrium adsorption capacities than the PAA hydrogel, indicating the beneficial effect of MAPTAC functionalization.

The Langmuir model provided the best fit for the PAA hydrogel for both Pb^{2+} and Cd^{2+}, suggesting that adsorption predominantly occurs as a monolayer on relatively homogeneous active sites. In contrast, the Freundlich model provided the best fit for the M10 hydrogel for both Pb^{2+} and Cd^{2+}, indicating adsorption on a heterogeneous surface with sites of different energies. The Freundlich constants ($n > 1$) indicate favorable adsorption on a heterogeneous surface. The Temkin model showed moderate agreement with the experimental data, whereas the D–R model exhibited

the poorest fit. The Sips model also provided a satisfactory description of the adsorption equilibrium, yielding correlation coefficients close to those of the Freundlich model for the MAPTAC-modified hydrogel and the Langmuir model for PAA sample. For PAA, n values close to unity suggest relatively homogeneous adsorption, whereas lower n values for M10 indicate greater surface heterogeneity after MAPTAC modification. Overall, MAPTAC modification enhanced the adsorption capacity and increased surface heterogeneity through the introduction of additional nitrogen-containing functional groups.

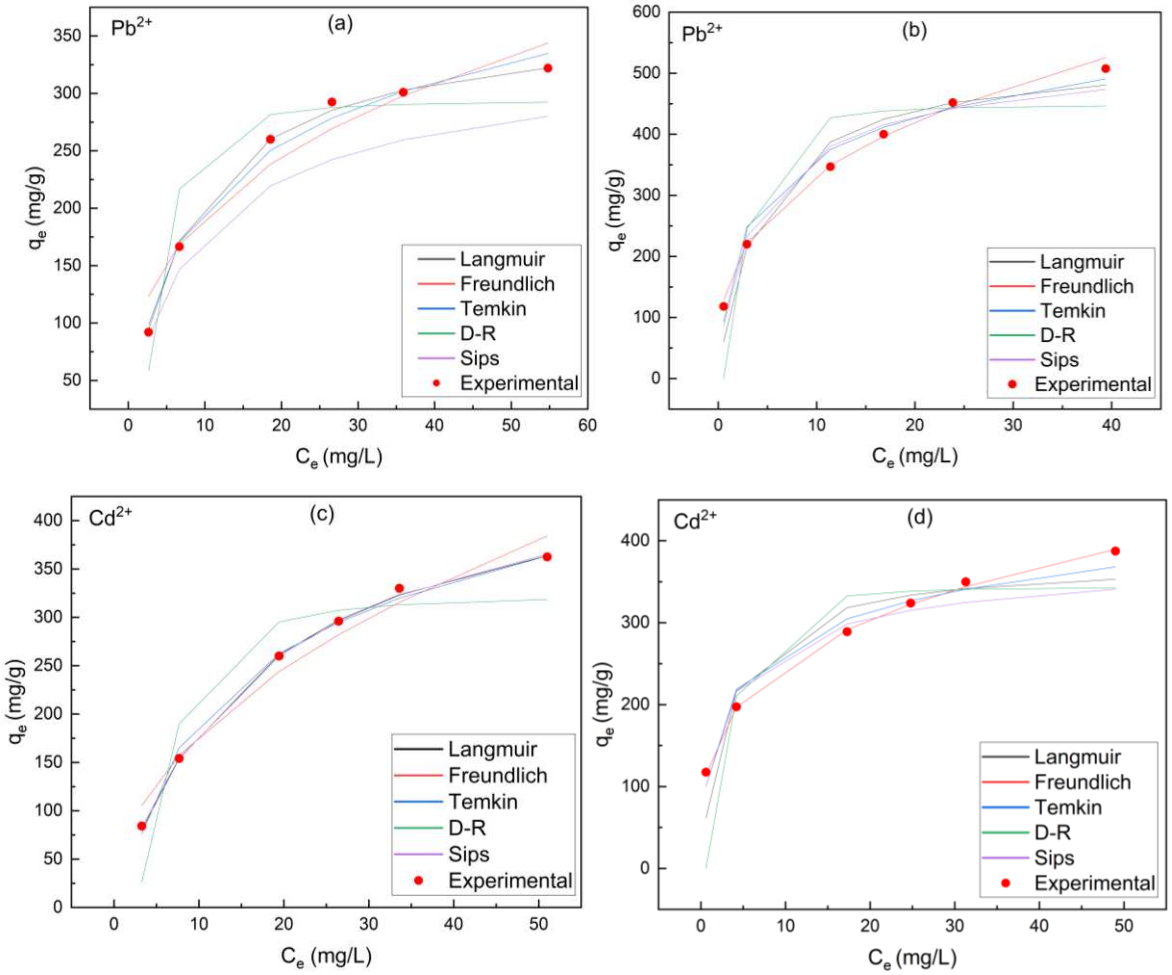


Fig. 12. Adsorption isotherms of Pb^{2+} and Cd^{2+} ions on (a, c) PAA and (b, d) M10 hydrogels.

Table 3. Isotherm parameters for Pb^{2+} and Cd^{2+} adsorption onto PAA and M10 hydrogels.

Hydrogel	Langmuir	Freundlich	Temkin

Metal ions		q_m (mg/g)	K_L	R^2	n	K_F	R^2	b_t	K_T	R^2
Pb^{2+}	PAA	366.98	0.13	0.995	2.95	88.79	0.927	31.8	1.34	0.916
	M10	532.94	0.23	0.954	3.03	156.48	0.991	26.63	4.94	0.927
Cd^{2+}	PAA	479.66	0.06	0.998	2.12	60.33	0.975	23.66	0.63	0.929
	M10	375.24	0.32	0.874	3.59	131.95	0.993	40.73	8.65	0.921

Metal ions	Hydrogel	D-R			Sips			
		q_m (mg/g)	B	R^2	n	K_S	q_m (mg/g)	R^2
Pb^{2+}	PAA	293.92	2.55×10^{-6}	0.888	0.84	0.15	343.82	0.905
	M10	448.41	1.13×10^{-6}	0.783	0.71	0.30	510.23	0.971
Cd^{2+}	PAA	322.75	5.76×10^{-6}	0.852	0.94	0.06	480.67	0.981
	M10	344.31	1.76×10^{-6}	0.631	0.64	0.46	400.21	0.974

3.9. Adsorption Kinetics

Figure 13 presents the fitting results for the adsorption of Pb^{2+} and Cd^{2+} ions onto PAA and M10 using various kinetic models, while the corresponding parameters are summarized in Table 4. Among the investigated models, the PSO model provided the best fit to the experimental data, with good agreement between the calculated and experimental adsorption capacities. These results suggest that chemisorption is likely the dominant adsorption mechanism, involving strong interactions between metal ions and the functional groups of the hydrogel. The modified M10 sample exhibited consistently higher equilibrium adsorption capacities than pristine PAA for both Pb^{2+} and Cd^{2+} ions, highlighting the beneficial effect of the additional amino-containing functional groups introduced by MAPTAC (Alkhaldi et al. 2026). The Weber–Morris model showed a lower goodness of fit, and the nonzero intercepts indicated that the fitted lines did not pass through the origin. Therefore, intraparticle diffusion contributes to the adsorption process but is not the sole rate-controlling step, suggesting that film diffusion and surface adsorption also contribute to the overall adsorption rate. The Elovich model provided a good fit, supporting the presence of energetically heterogeneous adsorption sites on both hydrogels. Collectively, the kinetic analyses indicate that adsorption proceeds through multiple steps, with chemisorption playing the dominant role while intraparticle diffusion contributes to, but does not solely control, the overall adsorption process (Ibrahim et al. 2012).

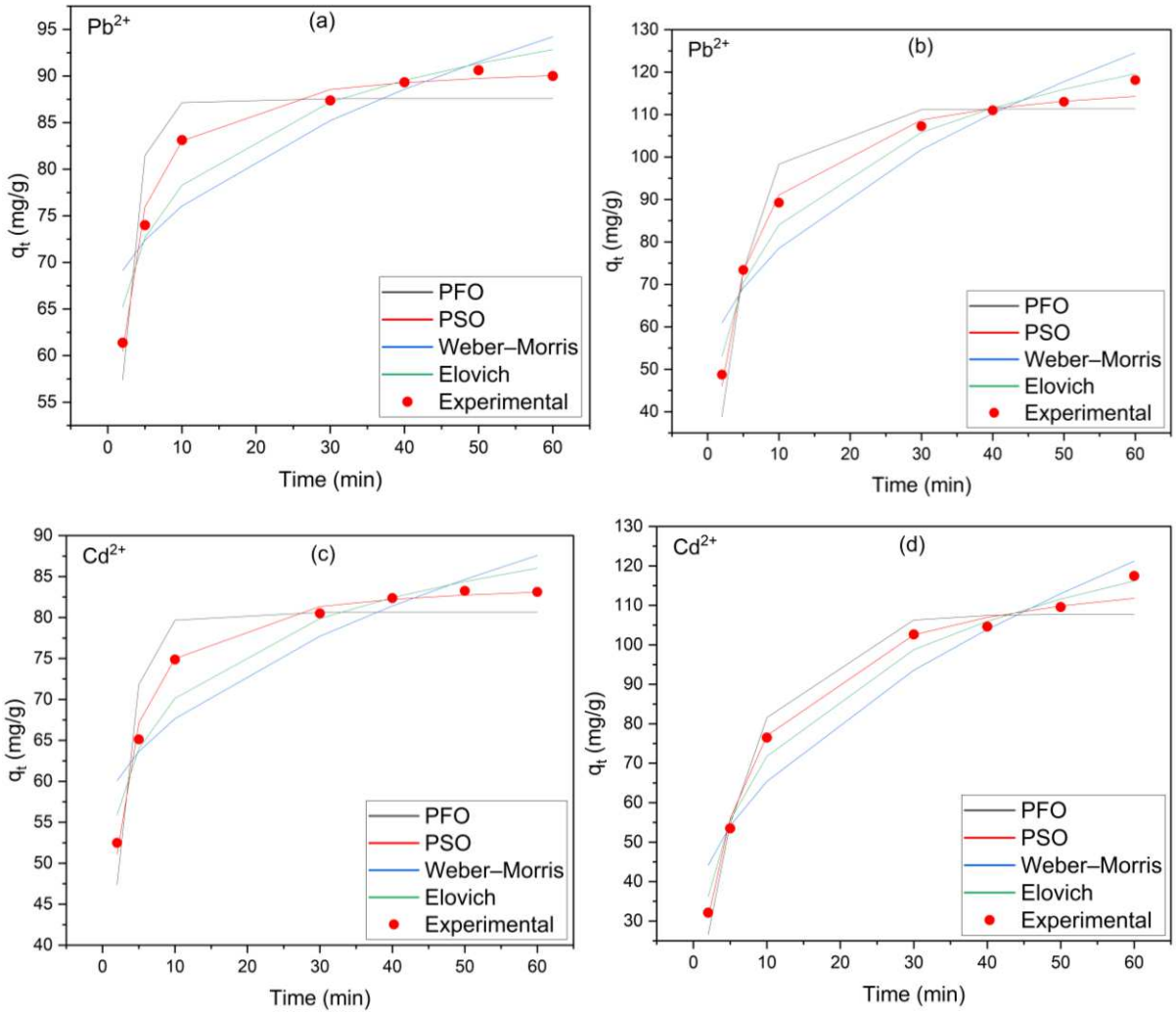


Fig. 13. Adsorption kinetics of Pb^{2+} and Cd^{2+} ions on (a, c) PAA and (b, d) M10 hydrogels.

Table 4. Kinetic parameters for the adsorption of Pb^{2+} and Cd^{2+} ions onto PAA and M10 hydrogels based on various kinetic models.

Metal ions	Hydrogel	PFO				PSO			
		$q_{e,exp}$	$q_{e,cal}$	K_1	R^2	$q_{e,exp}$	$q_{e,cal}$	K_2	R^2
Pb^{2+}	PAA	92.00	87.57	0.53	0.851	92.00	91.59	0.010	0.982
	M10	118.12	111.34	0.21	0.927	118.12	119.26	0.002	0.993
Cd^{2+}	PAA	84.12	80.63	0.44	0.861	84.12	84.42	0.008	0.990
	M10	117.46	107.84	0.14	0.967	117.46	119.02	0.001	0.985

Metal ions	Hydrogel	Weber–Morris			Elovich		
		C	K_{id}	R^2	α	β	R^2
Pb^{2+}	PAA	63.52	3.96	0.807	12474.3	0.12	0.924
	M10	46.73	10.04	0.914	131.53	0.04	0.985
Cd^{2+}	PAA	53.92	4.34	0.840	2421.0	0.11	0.951
	M10	26.92	12.17	0.924	39.94	0.03	0.973

3.10. Thermodynamics

The temperature-dependent adsorption behavior (Fig. 11) was consistent with the two linear regions observed in the Van't Hoff plot at 298 K. Therefore, the thermodynamic parameters were determined separately for the low- and high-temperature regions.

In the lower temperature range (278–298 K, Table 5), positive ΔH° values were obtained for all adsorption systems, suggesting an apparent endothermic behavior. This trend may be associated with enhanced hydrogel swelling and improved accessibility of internal adsorption sites, possibly accompanied by partial dehydration of hydrated metal ions prior to adsorption (Liang et al. 2026). The positive ΔS° values further suggest increased disorder at the solid–solution interface during adsorption (Liang et al. 2026). As a result, adsorption capacity and K increased with temperature in this region.

Table 5. Thermodynamic properties of Pb^{2+} and Cd^{2+}adsorption on PAA and PAA-MAPTAC hydrogels (T ≤ 298).

Metal ions	Hydrogel	ΔH° (kJ/mol)	ΔS° (J/mol.K)	T(K)	ΔG° (kJ/mol)	K
Pb^{2+}	PAA	23.08	164.49	278	-22.63	17839.81
				288	-24.34	25961.54
				298	-25.91	34848.48
	M10	30.26	203.55	278	-26.34	89126.02

				288	-28.30	136309.50
				298	-30.41	214772.70
Cd^{2+}	PAA	17.65	143.35	278	-22.18	14733.12
				288	-23.65	19551.28
				298	-25.04	24591.99
	M10	43	245.37	278	-25.26	55806.01
				288	-27.56	100112.61
				298	-30.17	194796.85

At 298 K, the highest K values and the most favorable adsorption capacities were observed, indicating an optimal balance between mass-transfer efficiency and adsorption affinity. Consequently, this temperature was identified as the optimum adsorption temperature for both Pb^{2+} and Cd^{2+} ions. In the higher temperature range (298–353 K, Table 6), the calculated ΔH° values became negative, indicating that the intrinsic adsorption process is exothermic. Consistent with this behavior, K decreased with increasing temperature, suggesting a gradual shift of the adsorption equilibrium toward desorption. Although ΔS° remained positive, its lower magnitude compared with that in the lower-temperature region suggests a reduced entropic contribution to the adsorption process. These findings suggest that once diffusion and swelling limitations are overcome, the intrinsic thermodynamic nature of adsorption becomes dominant. The negative ΔG° values obtained at all temperatures indicate that the adsorption process is thermodynamically spontaneous over the investigated temperature range. Moreover, the M10 hydrogel consistently exhibited more negative ΔG° values and higher K values than pristine PAA, demonstrating stronger thermodynamic affinity and more favorable interactions with Pb^{2+} and Cd^{2+} ions. Overall, the thermodynamic analysis demonstrates that MAPTAC modification enhances the spontaneity and thermodynamic affinity of Pb^{2+} and Cd^{2+} adsorption, while the experimental temperature study identifies 298 K as the optimum operating temperature.

Table 6. Thermodynamic properties of Pb^{2+} and Cd^{2+} adsorption on PAA and PAA-MAPTAC hydrogels (T ≥ 298).

Metal ions	Hydrogel	ΔH° (kJ/mol)	ΔS° (J/mol.K)	T(K)	ΔG° (kJ/mol)	K
Pb^{2+}	PAA	-17.57	27.82	298	-25.91	34848.48
				313	-26.26	24156.89
				333	-26.74	15653.15
				353	-27.48	11649.92
	M10	-21.41	29.89	298	-30.41	214772.70

				313	-30.69	132848.80
				333	-31.23	79411.76
				353	-32.09	56181.32
Cd^{2+}	PAA	-11.95	43.92	298	-25.04	24591.99
				313	-25.69	19387.76
				333	-26.60	14912.28
				353	-27.45	11538.46
	M10	-17.24	43.21	298	-30.17	194796.85
				313	-30.66	131178.16
				333	-31.71	94337.61
				353	-32.48	64187.12

Adsorption Mechanism

Based on the FT-IR, zeta potential, pH-dependent adsorption, and equilibrium results, a schematic representation of the proposed adsorption mechanism is presented in Fig. 14. The proposed mechanism suggests that Pb(II) and Cd(II) adsorption involves a combination of metal–ligand interactions and electrostatic attraction within the polymer network. In M10, MAPTAC incorporation provides additional oxygen-containing functional sites that may contribute to metal-ion binding, while the carboxylate groups of the PAA network remain important adsorption sites. These proposed interactions are consistent with the observed spectral changes and the enhanced adsorption performance of M10.

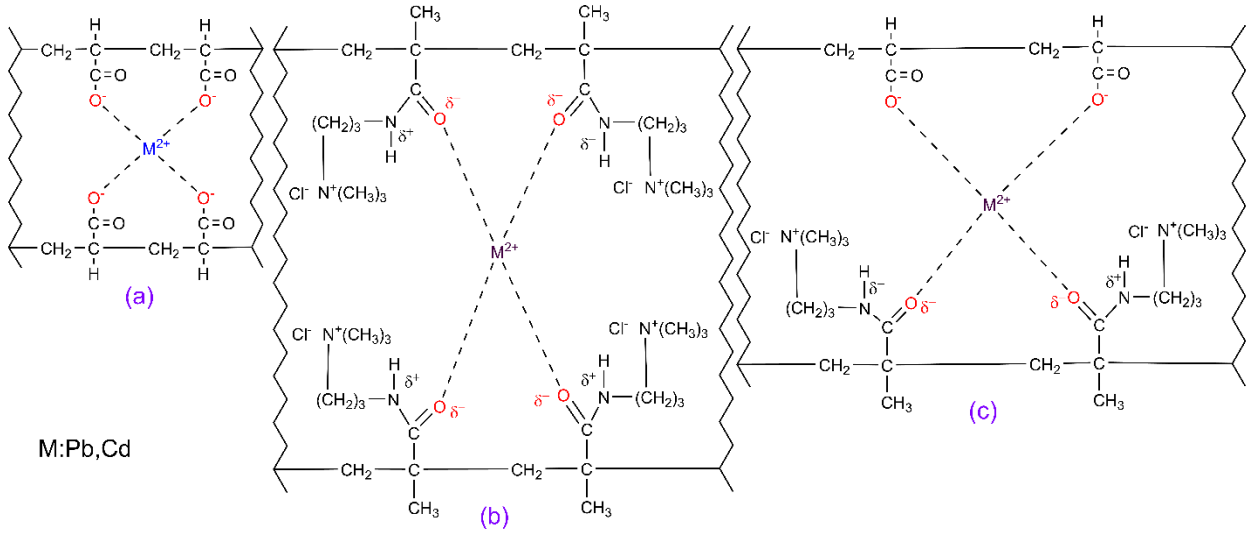


Fig. 14. Schematic representation of the proposed interactions of Pb^{2+} and Cd^{2+} ions with functional groups in (a) PAA, (b) MAPTAC, and (c) M10 hydrogels.

4. Conclusion

In this study, a poly(acrylic acid-co-sodium acrylate) superabsorbent hydrogel was successfully modified with MAPTAC to enhance its adsorption performance toward Pb^{2+} and Cd^{2+} ions. Among the synthesized materials, the hydrogel containing 10 g MAPTAC exhibited the best overall performance and was selected for further characterization and adsorption studies. Under the optimum conditions, the M10 hydrogel achieved removal efficiencies of 94.5% for Pb^{2+} and 93.97% for Cd^{2+}. Characterization confirmed the incorporation of MAPTAC into the polymer network, resulting in improved structural stability, AUL, and surface charge properties. Isotherm analysis showed that pristine PAA followed the Langmuir model, whereas the M10 sample was better described by the Freundlich model, indicating increased surface heterogeneity after MAPTAC modification. The corresponding maximum adsorption capacities reached 532.94 mg/g for Pb^{2+} and 375.24 mg/g for Cd^{2+}. Thermodynamic analysis confirmed the spontaneous nature of adsorption, with the modified hydrogel showing higher equilibrium constants and more negative ΔG° values than pristine PAA, indicating stronger adsorption affinity toward both metal ions. Overall, MAPTAC modification enhanced the adsorption performance and structural properties of the acrylate-based hydrogel, demonstrating its potential for Pb^{2+} and Cd^{2+} removal from contaminated water and industrial wastewater.

Statements and Declarations

Funding

This research received no external funding.

Authors' Contributions

Mahdi Taheri conducted the experiments, collected the data, and wrote the original draft of the manuscript. Masoud Vesali-Naseh, Alireza Sabzevari, and Kourosh Kabiri analyzed the experimental data and reviewed the manuscript.

Ethical Approval

Not applicable.

Consent to Participate

Not applicable.

Consent to Publish

Not applicable.

Competing Interests

The authors declare no competing interests.

Data Availability Statement

The datasets generated and analyzed during the current study are available from the corresponding author upon reasonable request.

Acknowledgements

Not applicable.

References

Abdipour A, Sobhani H, Vesali-Naseh M (2025) Preparation of graphene oxide-supported hydrogel adsorbent for Zn ions removal. Proc Inst Civ Eng Water Manag 95-104. https://doi.org/10.1680/jwama.22.00010

Alkhaldi HS, Baata M, Alhajri F, Elbasiony AM, Almoiqli MS, Madani M, Ghobashy MM (2026) Recent progress in the preparation and environmental applications of functionalized adsorbent hydrogel: a review. RSC Adv 16:7287-7336. https://doi.org/10.1039/D5RA07905E

Badsha MA, Khan M, Wu B, Kumar A, Lo IMC (2021) Role of surface functional groups of hydrogels in metal adsorption: from performance to mechanism. J Hazard Mater 408:124463. https://doi.org/10.1016/j.jhazmat.2020.124463

Behrendt F, Gottschaldt M, Schubert US (2024) Surface functionalized cryogels - characterization methods, recent progress in preparation and application. Mater Horiz 11:4600-4637. https://doi.org/10.1039/D4MH00315B

Chen F, Zhao Y, Zhao H, Zhou X, Liu X (2024) Heavy metal removal from wastewater using poly(gamma-glutamic acid)-based hydrogel. Gels 10:259. https://doi.org/10.3390/gels10040259

Darban Z, Shahabuddin S, Gaur R, Ahmad I, Sridewi N (2022) Hydrogel-based adsorbent material for the effective removal of heavy metals from wastewater: a comprehensive review. Gels 8:263. https://doi.org/10.3390/gels8050263

Deptula A, Rangel-Galera J, Espinosa-Marzal RM (2023) Control of surface morphology, adhesion and friction of colloidal gels with lamellar surface interactions. Adv Funct Mater 33:2300896

Fang L, Wang Y, Zhu Y, Li C, Cheng C, Liang T, Lv X, Yu H (2025) Cellulose hydrogel-based evaporator with integrated adsorption function for simultaneous water production and lead ion removal. Sep Purif Technol 136094. https://doi.org/10.1016/j.seppur.2025.136094

Fei J, Tang T, Zhou L, He H, Ma M, Shi Y, Chen S, Wang X (2023) High-toughness and biodegradable superabsorbent hydrogels based on dual functional crosslinkers. ACS Appl Polym Mater 5:3686-3697. https://doi.org/10.1021/acsapm.3c00348

Fei J, Tang T, Zhou L, He H, Ma M, Shi Y, Chen S, Wang X (2024) Swelling behavior of sodium lignosulfonate grafted polyacrylic acid highly absorbent hydrogels with two-phase structure. Polymer 300:126828. https://doi.org/10.1016/j.polymer.2024.126828

Foo KY, Hameed BH (2010) Insights into the modeling of adsorption isotherm systems. Chem Eng J 156:2-10. https://doi.org/10.1016/j.cej.2009.09.013

Furtado LM, Yee M, Fernandes R, Valera TS, Itri R, Petri DF (2023) Rheological and mechanical properties of hydroxypropyl methylcellulose-based hydrogels and cryogels controlled by AOT and SDS micelles. J Colloid Interface Sci 648:604-615. https://doi.org/10.1016/j.jcis.2023.06.014

Hu T, Zhang M, Wei X, Xu Z, Li D, Deng J, Li Y, Zhang Y, Lin X, Wang J (2024) Efficient Pb(II) removal from contaminated soils by recyclable, robust lignosulfonate/polyacrylamide double-network hydrogels embedded with Fe_2O_3 via one-pot synthesis. J Hazard Mater 479:135712. https://doi.org/10.1016/j.jhazmat.2024.135712

Ibrahim HS, Ammar NS, Soylak M, Ibrahim M (2012) Removal of Cd(II) and Pb(II) from aqueous solution using dried water hyacinth as a biosorbent. Spectrochim Acta A 96:413-420. https://doi.org/10.1016/j.saa.2012.05.039

Kato S, Kansha Y (2024) Comprehensive review of industrial wastewater treatment techniques. Environ Sci Pollut Res 31:51064-51097. https://doi.org/10.1007/s11356-024-34584-0

Kim HC, Kwon YR, Kim JS, Kim JH, Kim DH (2023) Superabsorbent polymer with enhanced gel strength and heat resistance using itaconic acid-based oligomer. Polym Adv Technol 34:2564-2572. https://doi.org/10.1002/pat.6072

Liang L, Cao X, Pan H, Sun J, Luo T, Liu X (2026) Advanced chitosan-based hydrogels for efficient removal of Pb(II) from aqueous solutions: adsorption performance and mechanism insights. Environ Sci Eur 38:79. https://doi.org/10.1186/s12302-026-01342-7

Linder TG, Heinzelmann A, Kamphus J, Seiffert S (2024) Influence of the crosslinker hydrophobicity on the swelling kinetics of poly(acrylic acid) microgels. Macromol Chem Phys 225:2400138. https://doi.org/10.1002/macp.202400138

Liu T, Jiao C, Peng X, Chen YN, Chen Y, He C, Liu R, Wang H (2018) Super-strong and tough poly(vinyl alcohol)/poly(acrylic acid) hydrogels reinforced by hydrogen bonding. J Mater Chem B 6:8105-8114. https://doi.org/10.1039/c8tb02556h

Lu L, Liu Z, Zheng Q, Qian Z, Yue C, Song L, Zhou Q, Liu F (2026) Green composite hydrogel coupling regulated with waste aluminum sludge and biomass for highly selective Pb(II) removal. J Hazard Mater 505:141478. https://doi.org/10.1016/j.jhazmat.2026.141478

Lu X, Liu J, Gao L, Zhang J, Yan X, Ma B, Xia W (2026) Review on MnO_2-based adsorbents for removal and recovery of metal ions from complex solution. Sustain Mater Technol e02047. https://doi.org/10.1016/j.susmat.2026.e02047

Mohammadbagheri Z, Rahmati A, Saeedi S, Movahedi B (2024) Bio-based nanocomposite hydrogels derived from poly(glycerol tartrate) and cellulose: thermally stable and green adsorbents for efficient adsorption of heavy metals. Chemosphere 349:140956. https://doi.org/10.1016/j.chemosphere.2023.140956

Mohammed A, Mohammed C, Mautner A, Kistow M, Chaitram P, Bismarck A, Ward K (2024) On the performance of Sargassum-derived calcium alginate ion exchange resins for Pb2+ adsorption: batch and packed bed applications. Environ Sci Pollut Res 31:31224-31239. https://doi.org/10.1007/s11356-024-33314-w

Monroy-Licht A, Martinez-Burgos WJ, De Carvalho JC, Cavali M, Woiciechowski AL, Karp SG, Soccol CR, De la Parra-Guerra AC, Pozzan R, Acevedo-Barrios R (2025) Biological approaches to mitigate heavy metal pollution from battery production effluents: advances, challenges, and perspectives. Environ Sci Pollut Res 32:20844-20878. https://doi.org/10.1007/s11356-025-36792-8

Naderzadeh R, Vesali-Naseh M, Rezaeivala M (2026) Enhanced photocatalytic performance of mixed-phase TiO_2-RGO nanocomposite for fast methylene blue decomposition under visible light. Res Chem Intermed 52:47-62. https://doi.org/10.1007/s11164-025-05799-8

Rayat Pisheh H, Sabzevari A, Ansari M, Kabiri K (2025) Development of HEMA-succinic acid-PEG bio-based monomers for high-performance hydrogels in regenerative medicine. Biopolymers 116:e23631. https://doi.org/10.1002/bip.23631

Siahkamari M, Jamali A, Sabzevari A, Shakeri A (2017) Removal of lead(II) ions from aqueous solutions using biocompatible polymeric nano-adsorbents: a comparative study. Carbohydr Polym 157:1180-1189. https://doi.org/10.1016/j.carbpol.2016.10.085

Takeda N, Fukushi K, Okuyama A, Takahashi Y (2024) Solid-liquid partitioning and speciation of Pb(II) and Cd(II) on goethite under high pH conditions, as examined by subnanomolar heavy metal analysis, X-ray absorption spectroscopy, and surface complexation modeling. Chemosphere 363:142766. https://doi.org/10.1016/j.chemosphere.2024.142766

Usman M, Taj MB, Carabineiro SAC (2023) Gum-based nanocomposites for the removal of metals and dyes from waste water. Environ Sci Pollut Res 30:102027-102046. https://doi.org/10.1007/s11356-023-29389-6

Vesali-Naseh M, Barati A, Vesali Naseh MR (2019) Efficient copper removal from wastewater through montmorillonite-supported hydrogel adsorbent. Water Environ Res 91:332-339. https://doi.org/10.1002/wer.1047

Xu H, Ou Z, Li W, Hu T, Zhang Y, Xu H, Wang J, Li Y (2024) Cadmium(II) adsorption by recyclable zeolite-loaded hydrogel: extension to the removal of cadmium(II) from contaminated soil. Chem Eng J 492:151842. https://doi.org/10.1016/j.cej.2024.151842

Yang Z, Yang T, Yang Y, Yi X, Hao X, Xie T, Liao CJ (2021) The behavior and mechanism of the adsorption of Pb(II) and Cd(II) by a porous double network hydrogel derived from peanut shells. Mater Today Commun 27:102449. https://doi.org/10.1016/j.mtcomm.2021.102449

Zalyhina V, Cheprasova V, Belyaeva V, Romanovski V (2021) Pigments from spent Zn, Ni, Cu, and Cd electrolytes from electroplating industry. Environ Sci Pollut Res 28:32660-32668. https://doi.org/10.1007/s11356-021-13007-4

Zanbili F, Gozali Balkanloo P, Poursattar Marjani A (2025) Semi-IPN polysaccharide-based hydrogels for effective removal of heavy metal ions and dyes from wastewater: a comprehensive investigation of performance and adsorption mechanism. Rev Environ Health 40:296-318. https://doi.org/10.1515/reveh-2024-0004

Zhao D, Deng H, Wang W, Hu L, Ye S, Fu J, Zhang S (2025) Synthesis, characterization and adsorption of Pb(II), Cd(II) and Cu(II) by red mud/polyacrylic acid/sodium carboxymethyl cellulose hydrogel. Arab J Chem 18:106067. https://doi.org/10.1016/j.arabjc.2024.106067